

Heat distribution in materials

Elling Svee, Anthony Schøyen, Mathias Karsrud Nordal

1 Introduction

Heat distribution in anisotropic materials can be modeled in the same way as in isotropic materials. However, in the anisotropic case the heat conductivity is not the same in every direction. In this project we will be considering the heat distribution in the solid Ω , with heat conductivity κ and internal heat source f . The model that we will be using is derived from the conservation of energy, as well as Fourier's law for the heat flux. Moreover, we assume the system to be stationary, i.e. $\partial_t T = 0$. This results in the following model:

$$-\nabla \cdot (\kappa \nabla T) = f \quad \text{in } \Omega \quad \partial \Omega = g \quad (1)$$

Firstly we consider an anisotropic solid, where $\mathbf{d}_1 = (1, 0)$ and $\mathbf{d}_2 = (1, r \in \mathbb{R})$, are two distinguished directions for heat flow. These directions defines the heat conductivity $\kappa = \begin{pmatrix} a+1 & r \\ r & r^2 \end{pmatrix}$ where $a > 0$. We will study the following system in a rectangular domain

$$\nabla \cdot (\kappa \nabla T) = (a+1)\partial_x^2 u + 2r\partial_x \partial_y u + r^2 \partial_y^2 u = a\partial_x^2 u + (\mathbf{d}_2 \cdot \nabla)^2 u \triangleq \mathcal{L}u \quad (2)$$

In addition we will investigate the same equation assuming isotropic behavior, i.e. $\kappa = I$, on an irregular domain. The equation of interest (1) simplifies to the Poisson equation $\Delta u = \partial_x^2 u + \partial_y^2 u = -f$. Our domain Ω is the first quadrant under the curve $\gamma_3 = \{(x, 1-x^2) | x \in [0, 1]\}$ so near the right and up-border, the rectangular grid won't work. We tried two different methods to solve this problem, fattening the boundary (FTB) and modifying the discretization near the boundary (MTD).

2 Numerical Model

2.1 Rectangular Domain

Let $\Omega = [0, 1] \times [0, 2]$ and consider a grid $\bar{\mathbb{G}} = \partial \mathbb{G} \cup \mathbb{G}$ with step size $h = \frac{1}{M}$ ($M \in \mathbb{N}$) and $k = |r|/h$ in the x and y directions respectively. In order to solve the system in Ω we will approximate problem (2) using central differences in the \mathbf{d}_1 and \mathbf{d}_2 directions. Discretization of the first term in (x_m, y_n) is done in the usual manner, that is:

$$a\partial_x^2 u_m^n \approx a \left[\frac{U_{m+1}^n - 2U_m^n + U_{m-1}^n}{h^2} \right] \quad (3)$$

The discretization of the directional derivative in (x_m, y_n) , is obtained in the following way:

$$(\mathbf{d}_2 \cdot \nabla)^2 u_m^n = \partial_x^2 u + 2r\partial_x \partial_y u_m^n + r^2 \partial_y^2 u_m^n \approx \alpha U_{m+1}^{n+1} + \beta U_m^n + \gamma U_{m-1}^{n-1} \quad (4)$$

For convenience we display some common Taylor expansions:

$$\begin{aligned} u_{m \pm 1}^{n \pm 1} &= u_m^n \pm h(u_x)_m^n \pm k(u_y)_m^n + \frac{1}{2}h^2(u_{xx})_m^n + hk(u_{xy})_m^n + \frac{1}{2}k^2(u_{yy})_m^n + \sum_{l=3}^{\infty} \frac{(\text{sgn}(\pm))^l}{l!} \sum_{i=0}^l \binom{l}{i} \frac{\partial^l u_m^n}{\partial x^i \partial y^{l-i}} h^i k^{l-i} \\ u_{m \pm 1}^n &= u_m^n \pm h(u_x)_m^n + \frac{1}{2}h^2(u_{xx})_m^n + \sum_{l=3}^{\infty} \frac{(\text{sgn}(\pm))^l}{l!} \frac{\partial^l}{\partial x^l} u_m^n h^l \end{aligned} \quad (5)$$

Taylor expanding $U_{m\pm 1}^{n\pm 1}$ about u_m^n results in:

$$\begin{aligned}\alpha u_{m+1}^{n+1} + \beta u_m^n + \gamma u_{m-1}^{n-1} &= (\alpha + \beta + \gamma)u_m^n + (\alpha - \gamma)h(u_x)_m^n + (\alpha - \gamma)k(u_y)_m^n + \frac{1}{2}(\alpha + \gamma)h^2(u_{xx})_m^n \\ &\quad + (\alpha + \gamma)hk(u_{xy})_m^n + \frac{1}{2}(\alpha + \gamma)k^2(u_{yy})_m^n + O(h^3)\end{aligned}\tag{6}$$

We must define α, β and γ , such that subtracting (6) from (4) yields the highest possible precision. Hence, we must have:

$$\begin{aligned}\alpha - \gamma &= 0, \implies \alpha = \gamma \\ \alpha + \beta + \gamma &= 0, \implies \beta = -2\alpha \\ \frac{1}{2}(\alpha + \gamma)h^2 &= 1, \implies \alpha = \gamma = \frac{1}{h^2} \implies \beta = -\frac{2}{h^2}\end{aligned}$$

Observe that $\frac{1}{2}(\alpha + \gamma)hk = 2|r|$ and $\frac{1}{2}(\alpha + \gamma)k^2 = r^2$.

Moreover, the problem can be discretized as such:

$$-\mathcal{L}_h U_m^n = \frac{2}{h^2}(a+1)U_m^n - \frac{a}{h^2}(U_{m+1}^n + U_{m-1}^n) - \frac{1}{h^2}(U_{m+1}^{n+1} + U_{m-1}^{n-1}) = f_m^n\tag{7}$$

This can further be expressed on vector form as $A_h \mathbf{U} = h^2 \mathbf{f} + \mathbf{g}$ where $A_h = \text{blocktridiag}\{-L_{M-1}, B, -U_{M-1}\}$. In (7), U_{M-1} and L_{M-1} denotes the $(M-1) \times (M-1)$ upper and lower shifting matrices respectively. Furthermore, $B = \text{tridiag}\{-a, 2(a+1), -a\} \in \mathcal{M}_{(M-1) \times (M-1)}(\mathbb{R})$.

The stencil of the scheme can be seen in the appendix.

2.2 Irregular Domain

2.2.1 Fattening the Boundary

Using the finite difference method to estimate the double derivatives we get the usual five point formula:

$$-\mathcal{L}_h U_m^n = \frac{U_{m+1}^n - 2U_m^n + U_{m-1}^n}{h^2} + \frac{U_m^{n+1} - 2U_m^n + U_m^{n-1}}{h^2} = \frac{1}{h^2}(U_{m+1}^n + U_{m-1}^n + U_m^{n+1} + U_m^{n-1} - 4U_m^n) = f_m^n\tag{8}$$

When fattening the boundary on the irregular boundary, we assume that the boundary nodes inherits their value from their closest point. An illustration of this can be found in the appendix. For our curve, the closest point is given by $(r, 1 - r^2)$ where r is the real positive solution to $x_p + r(1 - 2y_p) - 2r^3 = 0$. The stencil is preserved for this method.

2.2.2 Modifying the Discretization near Boundary

When modifying the discretization, we assume that there are gridpoints on the boundary such that the lattice structure is semi preserved. That is, boundary nodes have an x or y -coordinate matching the original grid. See appendix for illustration. When using MTD, the five point formula will alter slightly.

Assume that the steplengths towards east and north are h_E and h_N respectively. We get:

$$\begin{aligned}\partial_x^2 u &= au(x + h_E) + bu(x) + cu(x - h) \approx a \left(u_m^n + h_E(u_x)_m^n + \frac{h_E^2}{2}(u_{xx})_m^n \right) + bu_m^n + a(u_m^n - h(u_x)_m^n + \frac{h^2}{2}(u_{xx})_m^n) \\ &= (a + b + c)u_m^n + (ah_E - ch)(u_x)_m^n + \left(\frac{ah_E^2 + ch^2}{2} \right) (u_{xx})_m^n \\ \implies a + b + c &= 0, \quad ah_E - ch = 0, \quad \frac{ah_E^2 + ch^2}{2} = 1 \\ \implies a &= \frac{2}{h^2} \frac{1}{\left(\frac{h_E}{h} + 1 \right) \frac{h_E}{h}}, b = -\frac{2}{h^2} \frac{1}{\frac{h_E}{h}}, c = \frac{2}{h^2} \frac{1}{\left(\frac{h_E}{h} + 1 \right)}\end{aligned}$$

Giving the updated formula:

$$\Delta u \approx \frac{2}{h^2} \left(\frac{U_{m+1}^n}{\psi(\psi+1)} + \frac{U_{m-1}^n}{(\psi+1)} + \frac{U_m^{n+1}}{\phi(\phi+1)} + \frac{U_m^{n-1}}{(\phi+1)} - \frac{(\psi+\phi)}{\psi\phi} U_m^n \right) \quad \psi = \frac{h_E}{h} \quad \phi = \frac{h_N}{h} \quad (9)$$

Observe that fixing $h_E, h_N = h$ yields the usual five point formula.

2.2.3 Implementation

For both methods we will utilize a quadratic grid, where A_h is constructed similarly as in the anisotropic instance.

$$A_h = \text{blocktridiag}\{-I_{M-1}, B, I_{M-1}\}, \quad B = \text{tridiag}\{-1, 4, -1\}$$

A minor modification is how we temporarily delete the nodes non-resident in the interior. After solving this "smaller" system, we simply fill up the missing nodes with 0's to regain the quadratic structure.

3 Analysis

3.1 Monotonicity

Definition 3.1.1: A scheme of the form

$$-\mathcal{L}_h U_P = \alpha_{PP} U_P - \sum_{Q \neq P} \alpha_{PQ} U_Q, \quad P \in \mathbb{G}, \quad Q \in \mathbb{G} \cup \partial\mathbb{G} \triangleq \overline{\mathbb{G}}$$

is said to be monotone if the scheme has positive coefficients (A1) and is boundary connected (A2), i.e.:

$$\alpha_{PP} > 0, \quad \alpha_{PQ} \geq 0, \quad \alpha_{PP} \geq \sum_{Q \neq P} \alpha_{PQ} \quad (A1)$$

$$\forall P \in \mathbb{G} \quad \exists Q \in \partial^* \mathbb{G} \subseteq \partial\mathbb{G} \quad \text{and} \quad P_1, \dots, P_k \in \mathbb{G} \quad \text{s.t.} \quad \alpha_{PP_1}, \alpha_{P_1P_2}, \dots, \alpha_{P_kQ} \neq 0 \quad (A2)$$

Claim: Scheme (7) is monotone

Proof: The coefficients are:

$$\begin{aligned} \alpha_{PP} &= \frac{2}{h^2}(a+1), \\ \alpha_{PQ_1} &= \frac{a}{h^2} = \alpha_{PQ_2}, \\ \alpha_{PQ_3} &= \frac{1}{h^2} = \alpha_{PQ_4} \end{aligned}$$

Considering $a \in \mathbb{R}^{>0}$, all of the above expressions are positive real numbers. Moreover, $\sum_{Q \neq P} \alpha_{PQ} = 2\frac{a}{h^2} + 2\frac{1}{h^2} = \frac{2}{h^2}(a+1) = \alpha_{PP}$. Hence, (A1) holds. Lastly, since we are working in a rectangular grid with equidistant nodes, we have boundary connectivity. The claim follows. \square

We end this section with a theorem that will be of great importance later.

Theorem 1 (Discrete Maximum Principle): For any monotone scheme, i.e. (A1) and (A2) holds, we have the following implication:

$$-\mathcal{L}_h U_P \leq 0 \implies \max_{P \in \mathbb{G}} U_P \leq \max_{P \in \partial\mathbb{G}} U_P$$

The proof of the above theorem is omitted.

3.2 L^∞ -stability

Definition 3.2.1: For any f and solution U of our discrete problem with $U_P = 0, \forall P \in \partial\mathbb{G}$, the scheme is called stable with respect to the right hand side if there exist a constant $\zeta > 0$ independent of step sizes and right hand side, such that $\|U\|_\infty \leq \zeta \|f\|_\infty$.

The motivation behind this definition is to easily derive an error bound for the global error as a function of the local truncation error. Recall, that the global error, e , is zero at the boundary, and that it is the solution of the problem with right hand side $f = \tau$. τ being the local truncation error. Hence, if the scheme is stable with respect to the right hand side, a bound on e is only a constant factor away from a bound on τ . However, proving a scheme to be stable might not be such an easy task. Nevertheless, for monotone schemes, this can be done quite directly, if the prover possesses a supersolution of the problem.

Definition 3.2.2: A function ψ is called a *supersolution* of the problem if $\psi_P > 0$ and $-\mathcal{L}_h \psi_P \geq 1, \forall P \in \mathbb{G}$.

Claim: Scheme (7) is L^∞ -stable.

Proof: Firstly, one can easily draw an analogy to the Poisson equation, for which $\Phi(x) = \frac{1}{2}x(1-x)$ is a supersolution. We see that $\Phi > 0, \forall x \in (0, 1)$. Moreover, since Φ is only a function of x , the second order directional derivative coincide with the second order partial derivative with respect to x . i.e. $\partial_x^2 \Phi = (\mathbf{d}_2 \nabla)^2 \Phi = -1$. As a result we have: $\mathcal{L}\Phi = -(a+1) \implies -\mathcal{L}\Phi = a+1 > 1$. Following directly from the definition; Φ is a supersolution to problem (7). Further, let V_P be a solution of the problem with right hand side f_P , such that $V_P = 0$ for all $P \in \partial\mathbb{G}$. Let $W_P = V_P - \|f\|_\infty \Phi_P$. Now:

$$-\mathcal{L}_h W_P = -\mathcal{L}_h V_P - \|f\|_\infty (-\mathcal{L}_h \Phi_P) = f_P - \|f\|_\infty (-\mathcal{L}_h \Phi_P) \stackrel{-\mathcal{L}_h \Phi_P \geq 1}{\leq} 0$$

Applying **Theorem 1** we get:

$$\begin{aligned} V_P - \|f\|_\infty \Phi_P &\leq \max_{\partial\mathbb{G}} \{V_P - \|f\|_\infty \Phi_P, 0\} \stackrel{V_P=0, P \in \partial\mathbb{G}}{=} \max_{\partial\mathbb{G}} \{-\|f\|_\infty \Phi_P, 0\} \stackrel{\|f\|_\infty \Phi_P \geq 0}{=} 0 \\ &\implies V_P \leq \|f\|_\infty \Phi_P \leq \max_{\Omega} \Phi \|f\|_\infty \stackrel{C \triangleq \max_{\Omega} \Phi}{=} C \|f\|_\infty \end{aligned}$$

To bound the potential negative values of V , we define the bijection $(V_P, f_P) \xrightarrow{\gamma} (-V_P, -f_P)$ and obtain:

$$-V_P \leq C \|f\|_\infty = C \|f\|_\infty \implies \|V\|_\infty \leq C \|f\|_\infty$$

The claim follows. \square

3.3 Error Bound

Now since $-\mathcal{L}_h e_P = -\tau_P \implies \|e\|_\infty \leq C \|\tau\|_\infty$, we need a bound on $\|\tau\|_\infty$ to obtain a bound on $\|e\|_\infty$. Note that $C = \max_{\Omega} \Phi = \frac{1}{8}$. Further recall the definition of $\tau_P = -\mathcal{L}u_P - (-\mathcal{L}_h u_P)$, i.e. the error caused by one iteration of the scheme. For our problem the truncation error is:

$$\tau_m^n = -\mathcal{L}u_m^n - (-\mathcal{L}_h u_m^n) = a\partial_x^2 u_m^n + (\mathbf{d}_2 \cdot \nabla)^2 u_m^n - \frac{1}{h^2} [2(a+1)u_m^n - a(u_{m+1}^n + u_{m-1}^n) - (u_{m+1}^{n+1} + u_{m-1}^{n-1})]$$

Using (5) to Taylor expand the last four terms, one can derive an expression for τ_m^n

$$\tau_m^n = \frac{a+1}{12} h^2 (u_{xxxx})_m^n + \frac{4}{3} h^2 (u_{yyyy})_m^n + \frac{8}{3} h^2 (u_{xyyy})_m^n + 2h^2 (u_{xxyy})_m^n + \frac{2}{3} h^2 (u_{xxxy})_m^n + O(h^4) \quad (10)$$

Furthermore, this expression can be bounded to endow a bound on the global error.

$$\begin{aligned} |\tau_P| &\leq \frac{a+1}{12} h^2 \max_{\Omega} |u_{xxxx}|_P + \frac{4}{3} h^2 \max_{\Omega} |u_{yyyy}|_P + \frac{8}{3} h^2 \max_{\Omega} |u_{xyyy}|_P + 2h^2 \max_{\Omega} |u_{xxyy}|_P + \frac{2}{3} h^2 \max_{\Omega} |u_{xxxy}|_P \\ &\quad \Downarrow \\ \|\mathbf{e}\|_\infty &\leq \frac{1}{8} \left[\frac{a+1}{12} \max_{\Omega} |u_{xxxx}|_P + \frac{4}{3} \max_{\Omega} |u_{yyyy}|_P + \frac{8}{3} \max_{\Omega} |u_{xyyy}|_P + 2 \max_{\Omega} |u_{xxyy}|_P + \frac{2}{3} \max_{\Omega} |u_{xxxy}|_P \right] h^2 \end{aligned} \quad (11)$$

From the above bound, we see that for sufficiently smooth functions, i.e. $u \in C^4(\Omega)$, the scheme has a convergence rate of 2.

3.4 Choosing r arbitrarily

Now, introduce a grid with stepsizes $h = \frac{1}{M}$ and $k = |r|h$, where r can be irrational.

Claim: In the case where r is irrational, the steps in the y -direction will miss the boundary $y = 2$.

Proof: Assume r irrational and that 2 can be written as $2 = Nk = \frac{N|r|}{M}$ where $N, M \in \mathbb{N}$.

$$2 = N \frac{|r|}{M} \implies |r| = \frac{2M}{N} \not\in \mathbb{Q}$$

A contradiction, as r is assumed irrational. Thus the grid will miss the boundary at $y = 2$. \square

In order to overcome the problem of missing the boundary, it can be fattened in the y -direction. That is, if the location of the boundary does not hit the grid after discretizing, it is moved to the closest outer gridpoints. Then, after the discretization, the steps will be sure to hit the outer y -boundary, even when r is irrational.

3.5 Order of convergence for MTB

Claim: Modifying the scheme at the boundary, results in linear convergence.

Proof: Recall from section 2.2.2 that the coefficients in (9), is chosen such that the constant and linear terms of the Taylor expansions cancel. Hence, we are left with the following expression after expanding the terms around u_m^n .

$$\begin{aligned} \Delta u &\approx (u_{xx})_m^n + (u_{yy})_m^n + \frac{2}{h^2} \left(\frac{1}{3!} (\psi h)^3 \frac{(u_{xxx})_m^n}{\psi(\psi+1)} - \frac{1}{3!} (h)^3 \frac{(u_{xxx})_m^n}{(\psi+1)} + \frac{1}{3!} (\phi h)^3 \frac{(u_{yyy})_m^n}{\phi(\phi+1)} - \frac{1}{3!} (h)^3 \frac{(u_{xxx})_m^n}{(\phi+1)} + O(h^4) \right) \\ &= (u_{xx})_m^n + (u_{yy})_m^n + \frac{2}{3!} h \left(\psi^2 \frac{(u_{xxx})_m^n}{(\psi+1)} - \frac{(u_{xxx})_m^n}{(\psi+1)} + \phi^2 \frac{(u_{yyy})_m^n}{(\phi+1)} - \frac{(u_{xxx})_m^n}{(\phi+1)} + O(h^4) \right) \\ &= (u_{xx})_m^n + (u_{yy})_m^n + \frac{2}{3!} \varpi(u, \phi, \psi) h, \quad \varpi(u, \phi, \psi, h) \triangleq \psi^2 \frac{(u_{xxx})_m^n}{(\psi+1)} - \frac{(u_{xxx})_m^n}{(\psi+1)} + \phi^2 \frac{(u_{yyy})_m^n}{(\phi+1)} - \frac{(u_{xxx})_m^n}{(\phi+1)} + O(h^4) \end{aligned}$$

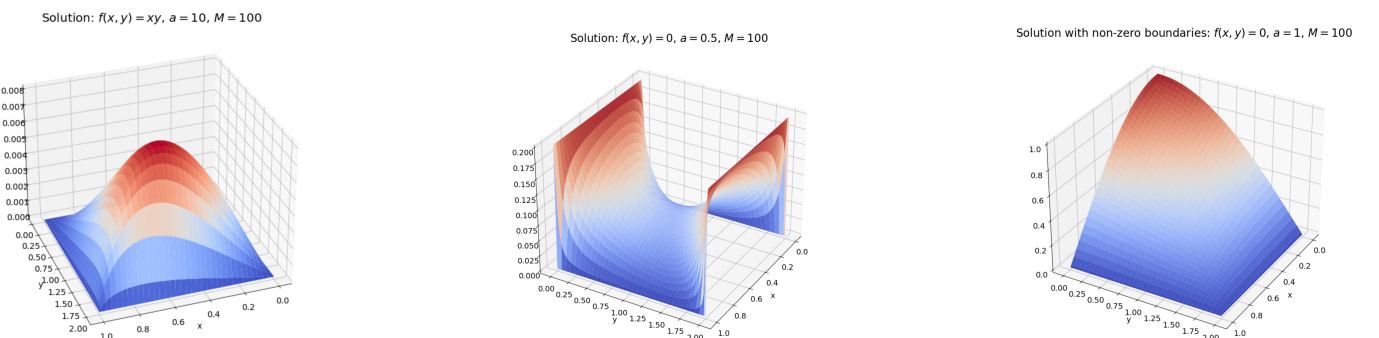
Consider the truncation error:

$$\tau_m^n = (u_{xx})_m^n + (u_{yy})_m^n - (u_{xx})_m^n - (u_{yy})_m^n - \frac{2}{3!} \varpi(u, \phi, \psi, h) h = O(h)$$

The claim follows. \square

Observe how $\psi = \phi = 1$ removes all linear terms making the usual five point formula $O(h^2)$, as we expect.

4 Verifying the numerical solver



Before comparing the numerical solver to exact solutions, it is nice practice to check that the solutions coincide with how we expect heat to distribute.

Observe from the solutions that in the cases when there are non-zero boundaries on two of the sides, the heat decreases steadily as we move towards the zero boundary's. This agrees with our intuition. Moreover, an internal heat source, f , gives a contribution over the entire surface. The highest temperature is not necessarily along the boundary, as we see in the leftmost plot. The size of the a -variable affects the relative strength of the conductivity in the d_1 and d_2 directions, with a larger a increasing the conductivity in the d_1 direction. Carefully inspecting the first plot shows how the temperature is barely shifted towards increasing x .

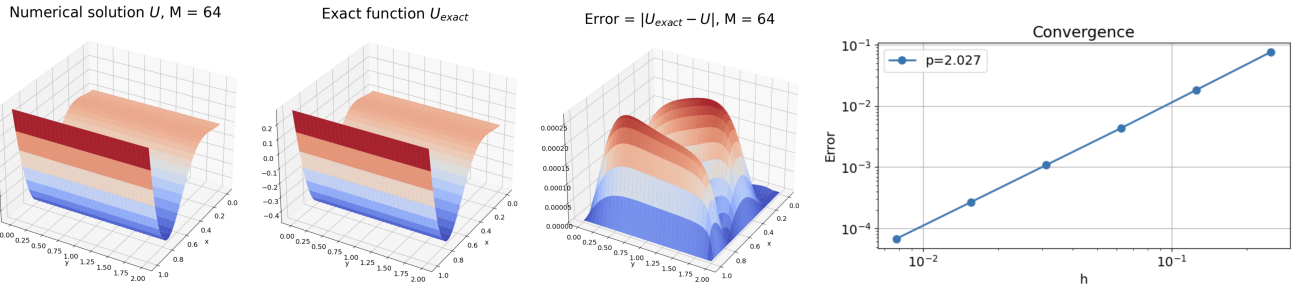
The solvers numerical solutions agrees with the expected behavior.

5 Results and Discussion

5.1 Anisotropic

5.1.1 Convergence rate

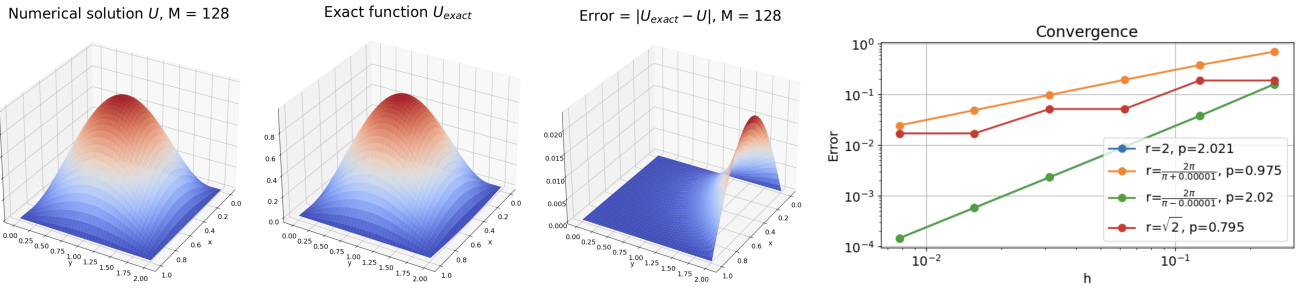
By modifying the right hand side f and the initial data in (1), the solver could find the exact solution in the lattice. Finding the larges value in the error array $\|e\|_\infty = |U_{\text{exact}} - U|$ for different stepsizes, we used linear regression to find the order of convergence. In the following plots the scheme has been solved using 6 different stepsizes. The test function is given $f(x, y) = x^2 \cos(5x)$.



The numerical and analytic solutions concurred very well. The general shapes are identical and the difference had an order magnitude equal -4 for $M = 64$. Moreover, the plots suggest a convergence rate of 2, which is consistent with the analysis.

5.1.2 Error when fattening for varying r

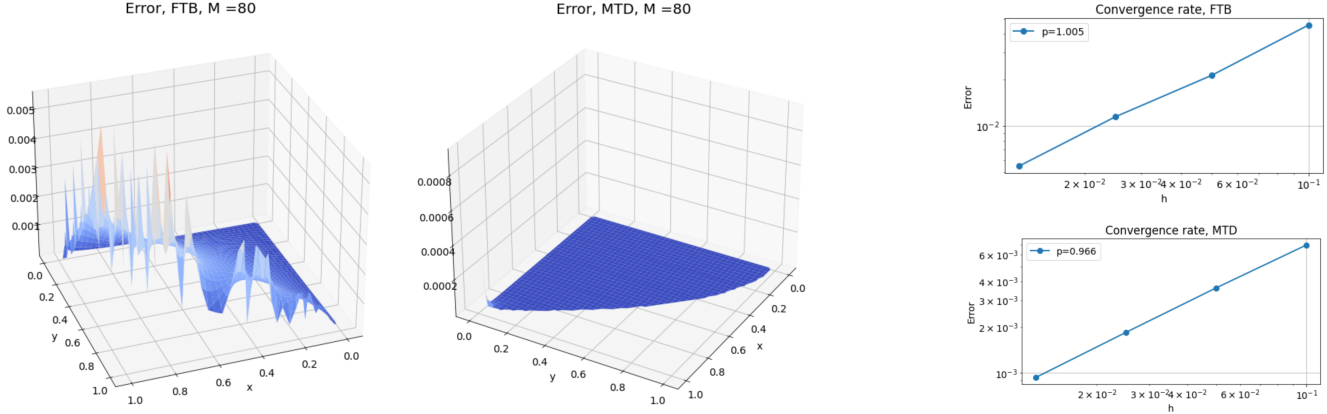
When fattening the boundary we also did a convergence test for different values of r . The test function is given by $f(x, y) = \sin(\pi x) \sin(\frac{\pi}{2}y)$



These plots suggests that the exact and numeric solution seems to somewhat disagree near the fattened boundary. The numerical and exact solution appear to align with the exception of the fattened boundary. Here, even for a function with zero on its boundaries, the numerical solution has a large error stemming from the boundary that had to be fattened.

The convergence rate are heavily dependent on r . Choosing two irrational r -values, slightly below and slightly above 2, yields completely different rate of convergence. In the case where r is below 2 we have to fatten the boundary a substantially larger distance than in the case where r is above 2. Observe from the convergence-plot that the scheme has a convergence rate $\approx 1, \approx 2$ respectively. In both these cases the grid is almost identical to the case of $r = 2$. Choosing an arbitrary r , it is hard to predict the exact convergence rate of the scheme as we get 0.8 for $r = \sqrt{2}$.

5.2 Isotropic



These plots demonstartes how both FTB and MTD gives an linear convergence in the uniform norm. The general accuracy of MTD was better as the order of magnitude of the error was lesser. Using $M = 80$, the error is around 10^{-2} for FTB whilst 10^{-3} for MTD.

Near the x and y -axis, the numeric and analytic solution agreed quite well.

The difference in spike behavior might be a consequence of how consistent the grid is in the different method. In FTB some boundary nodes will be closer to the original boundary than others. As we saw in the anisotropic fattening, the accuracy decreases with a bigger expansion. The spikes may be due to "unlucky" boundary points which are far from the original boundary. We see no such spikes in the MTD where the irregular grid is coherent with the boundary.

We got the impression that FTB was easier to implement. There is no need to update the stencil or the weighting in (9) as we do in MTD. Furthermore, in MTD some nodes are outside the lattice, which was a slight inconvenience.

For our implementation, MTD was faster, atleast for "small" M . When FTB, finding the closest boundary point required resolving a third degree polynomial, which was quite slow. For $M = 25$ the MTD is about 70 times faster. For a bigger M , say $M = 150$, their execution times were near even. Roughly speaking, the only difference in the solvers are solving the third degree polynomial in FTB versus 2 extra matrices in MTD. When we increase M the amount of polynomials increase linearly $\Theta(M)$. However, memory management for matrices increase quadratic $\Theta(M^2)$. This might explain the behaviors with the running times.

6 Conclusion

This work culminated in the study of how finite difference methods can be adapted to solve PDE's on irregular domains. The alterations of investigation, FTB and MTD, differs in how they handle boundary points.

A

Figures

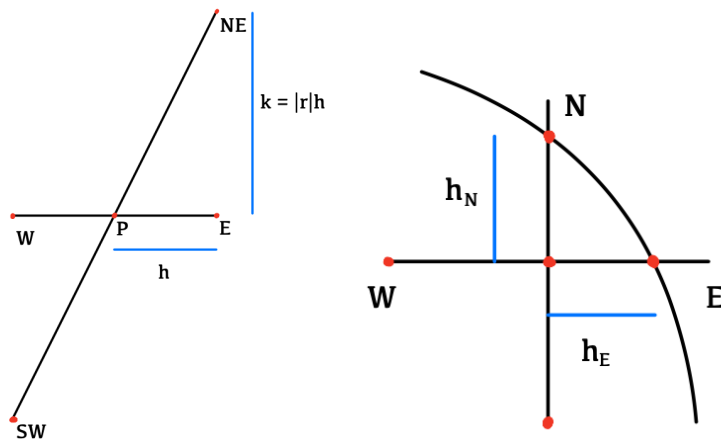


Figure 1: Stencil for scheme (7) Figure 2: Stencil for irregular grid

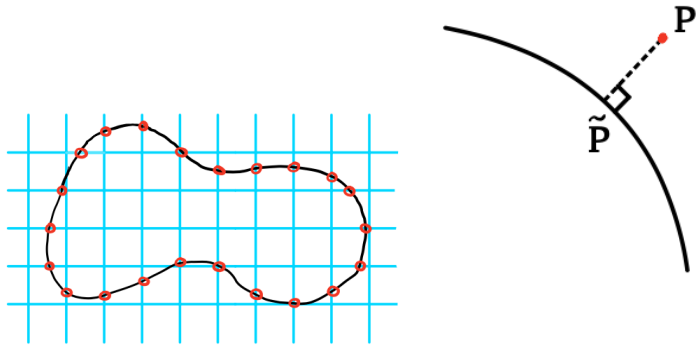


Figure 3: Irregular grid

Figure 4: Projection onto boundary